International Journal of Hyperthermia

ISSN: 0265-6736 (Print) 1464-5157 (Online) Journal homepage: https://www.tandfonline.com/loi/ihyt20

Polyethylene glycol-coated porous magnetic nanoparticles for targeted delivery of chemotherapeutics under magnetic hyperthermia condition

Ali Dabbagh, Ziba Hedayatnasab, Hamed Karimian, Masoud Sarraf, Chai Hong Yeong, Hamid Reza Madaah Hosseini, Noor Hayaty Abu Kasim, Tin Wui Wong & Noorsaadah Abdul Rahman

To cite this article: Ali Dabbagh, Ziba Hedayatnasab, Hamed Karimian, Masoud Sarraf, Chai Hong Yeong, Hamid Reza Madaah Hosseini, Noor Hayaty Abu Kasim, Tin Wui Wong & Noorsaadah Abdul Rahman (2018): Polyethylene glycol-coated porous magnetic nanoparticles for targeted delivery of chemotherapeutics under magnetic hyperthermia condition, International Journal of Hyperthermia, DOI: 10.1080/02656736.2018.1536809

To link to this article: https://doi.org/10.1080/02656736.2018.1536809

Published online: 14 Nov 2018.

INTERNATIONAL JOURNAL OF HYPERTHERMIA
https://doi.org/10.1080/02656736.2018.1536809

Taylor & Francis
Taylor & Francis Group

Polyethylene glycol-coated porous magnetic nanoparticles for targeted delivery of chemotherapeutics under magnetic hyperthermia condition

Ali Dabbagh[a,b], Ziba Hedayatnasab[c], Hamed Karimian[a], Masoud Sarraf[d], Chai Hong Yeong[a], Hamid Reza Madaah Hosseini[b], Noor Hayaty Abu Kasim[e,f], Tin Wui Wong[g] and Noorsaadah Abdul Rahman[h]

[a]School of Medicine, Faculty of Health and Medical Sciences, Taylor's University, Subang Jaya, Malaysia; [b]Department of Materials Science and Engineering, Sharif University of Technology, Tehran, Iran; [c]Department of Chemical Engineering, Faculty of Engineering, University of Malaya, Kuala Lumpur, Malaysia; [d]Department of Mechanical Engineering, Faculty of Engineering, University of Malaya, Kuala Lumpur, Malaysia; [e]Department of Restorative Dentistry, Faculty of Dentistry, University of Malaya, Kuala Lumpur, Malaysia; [f]Health and Well-being Research Cluster, Institute of Research Management and Services, University of Malaya, Kuala Lumpur, Malaysia; [g]Non-Destructive Biomedical and Pharmaceutical Research Centre, iPROMISE, Universiti Teknologi MARA, Puncak Alam, Selangor, Malaysia; [h]Department of Chemistry, Faculty of Science, University of Malaya, Kuala Lumpur, Malaysia

ABSTRACT

Purpose: Although magnetite nanoparticles (MNPs) are promising agents for hyperthermia therapy, insufficient drug encapsulation efficacies inhibit their application as nanocarriers in the targeted drug delivery systems. In this study, porous magnetite nanoparticles (PMNPs) were synthesized and coated with a thermosensitive polymeric shell to obtain a synergistic effect of hyperthermia and chemotherapy.

Materials and methods: PMNPs were produced using cetyltrimethyl ammonium bromide template and then coated by a polyethylene glycol layer with molecular weight of 1500 Da (PEG1500) and phase transition temperature of 48 ± 2 °C to endow a thermosensitive behavior. The profile of drug release from the nanostructure was studied at various hyperthermia conditions generated by water-bath, magnetic resonance-guided focused ultrasound (MRgFUS), and alternating magnetic field (AMF). The *in vitro* cytotoxicity and hyperthermia efficacy of the doxorubicin-loaded nanoparticles (DOX-PEG1500-PMNPs) were assessed using human lung adenocarcinoma (A549) cells.

Results: Heat treatment of DOX-PEG1500-PMNPs containing 235 ± 26 mg·g^{-1} DOX at 48 °C by water-bath, MRgFUS, and AMF, respectively led to 71 ± 4%, 48 ± 3%, and 74 ± 5% drug release. Hyperthermia treatment of the A549 cells using DOX-PEG1500-PMNPs led to 77% decrease in the cell viability due to the synergistic effects of magnetic hyperthermia and chemotherapy.

Conclusion: The large pores generated in the PMNPs structure could provide a sufficient space for encapsulation of the chemotherapeutics as well as fast drug encapsulation and release kinetics, which together with thermosensitive characteristics of the PEG1500 shell, make DOX-PEG1500-PMNPs promising adjuvants to the magnetic hyperthermia modality.

ARTICLE HISTORY
Received 10 November 2017
Accepted 12 October 2018

KEYWORDS
Magnetic nanoparticles; porous materials; thermosensitive nanocarriers; loading capacity; drug release

Introduction

Magnetite nanoparticles (MNPs) are promising agents for generation of a hyperthermia condition in the tumor tissue under exposure to the alternating magnetic fields (AMF) with clinically-relevant amplitudes [1]. These nanoparticles could also provide a synergistic effect of chemotherapy and hyperthermia when sufficient dosages of chemotherapeutics are conjugated on their surfaces. The drug-loaded MNPs could further be navigated through the body via external magnetic fields with appropriate driving forces to actively target the tumor site and release their cargo, while simultaneously produce a significant amount of thermal energy by different mechanisms such as hysteresis loss, Néel relaxation, Brown relaxation, and frictional losses [2–7].

In spite of the intrinsic advantages of MNPs, their limited loading capacity may result in insufficient drug dosages delivered to the tumor site [8–10]. Hence, synthesis of MNPs with porous structure is a particular solution to achieve higher drug loading capacities [11–13]. Moreover, MNPs could be coated by different thermosensitive agents to protect the encapsulated compounds from uncontrolled leakage [7,8,14–16]. When the particles reach the target tumor, the produced thermal energy dissociates the protective shell and facilitates release of the therapeutic load [17–19].

Recently, a new mechanism of thermal sensitivity has been introduced using low-melting point polymer nanoshells [8,14]. This research is an attempt to further enhance the drug release efficacy of this triggering mechanism using porous magnetic nanoparticles (PMNPs) as the drug reservoir core. As shown schematically in Figure 1, the controlled

CONTACT Ali Dabbagh ali.dabbagh@taylors.edu.my School of Medicine, Faculty of Health and Medical Sciences, Taylor's University, Subang Jaya, Malaysia

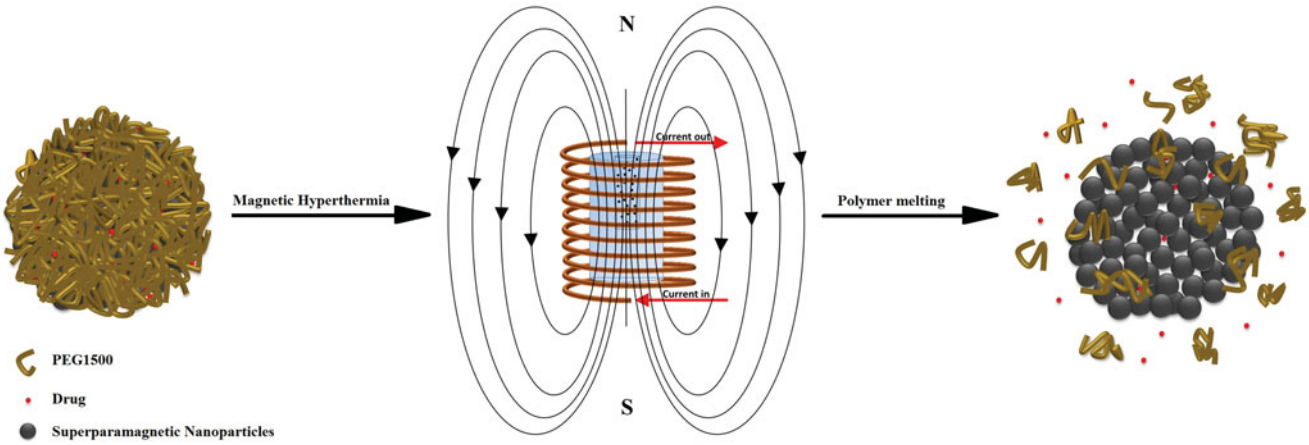

Figure 1. A schematic of the triggering mechanism from the porous core-shell nanostructures. Melting of the protective shell results in formation of preferred routes for controlled drug release.

synthesis parameters could endow agglomerated nanostructures with relatively high volumetric ratios of interparticle porosities. These nanostructures were further coated by a protective polyethylene glycol (PEG) shell with molecular weight of 1500 Da (PEG1500) and appropriate melting temperature in the hyperthermia range. It was assumed that the temperatures above the PEG1500 melting point (T_m) lead to partial removal of the protective shell and thus provide preferred trajectories for facilitated drug release. The AMF and magnetic resonance-guided focused ultrasound (MRgFUS) were employed as selected thermal modalities to evaluate the heating and drug release efficacies of these core-shell nanocarriers under exposure to different hyperthermia conditions.

Materials and methods

Synthesis of nanoparticles

PMNPs were synthesized by modification of the method described previously [20], where cetyl trimethyl ammonium chloride (CTAB) was added as a template to obtain nanoparticles with porous structure. In a typical procedure, 1 ml of ferrous sulfate heptahydrate ($FeSO_4.7H_2O$; 2M), 3.5 ml of ferric chloride ($FeCl_3$; 1M), and 500 mg of CTAB were thoroughly mixed in 25 ml of ultrapure water, followed by dropwise addition of 25 ml ammonium hydroxide (NH_4OH; 33%) under vigorous stirring. After 2 h, the nanoparticles were separated using a permanent magnet, washed with ethanol, and incubated in a methanol solution containing hydrochloric acid (HCl; 3%*v*/*v*) for 6 h to remove the CTAB template. The particles were again magnetically separated, rinsed with ethanol, and dried in 80 °C for 24 h.

The synthesis of PEG1500-PMNPs was carried out using the 'graft-to' method according to a previously described protocol [21]. Briefly, the surface-modified nanoparticles were firstly prepared by stirring the as-synthesized PMNPs and 3-aminopropyl triethoxysilane in toluene at 80 °C for 24 h. Then, the obtained particles were mixed with carboxyl-terminated PEG (COOH-PEG1500) in toluene at 80 °C for another 24 h. The synthesized nanoparticles were washed with ethanol and freeze-dried for 24 h to produce PEG1500-PMNPs with sufficient stability in aqueous solutions.

Characterizations

The phase structure of the synthesized nanoparticles was analyzed using X-Ray diffractometry technique (XRD; Philips PW1840, Amsterdam, the Netherlands) with Cu Kα radiation ($\lambda = 1.542$ A°), step size of 0.026°, and 2θ range of 20–70 degrees. The chemical composition of the core-shell nanoparticles was also investigated using Fourier transform infrared (FTIR; Nicolet 6700, ThermoScientific, Madison, WI) spectroscopy in the wavelength range of 600–4000 nm^{-1}.

The particles morphology and size were investigated using a transmission electron microscope (TEM; LEO Libra 120 kV, Carl Zeis AG, Oberkochen, Germany). Dynamic light scattering (Malvern Instruments, Malvern, UK) was employed to determine the size distribution of the produced particles as well as their zeta potential at pH 7.0. The surface area of the particles was also measured by Brunauer–Emmett–Teller approach (ASAP2020, TRISTAR II 3020 Kr, Micromeritics Instruments, Norcross, GA, USA). The magnetic characteristics of the synthesized nanoparticles were investigated using vibrated sample magnetometer (model 7400 series, Lakeshore, Chicago, IL). In order to calculate the onset phase transition temperature of PEG1500, differential scanning calorimetry (DSC820 with TSO 801RO robot, Mettler-Toledo, Columbus, OH, USA) with scan rate of 5 °C·min^{-1} was used. Thermogravimetric analysis (TGA; TGA/SDTA 851e, Mettler-Toledo, Greifensee, Switzerland) was also performed to calculate the weight percentage of the polymeric shell.

Drug loading

The drug loading capacity and drug release ratio were investigated using ultra-violet visible spectroscopy (UV-Vis; Shimadzu UV-1800, Shimadzu Corporation, Kyoto, Japan) at wavelength range of 260–600 nm [8,14]. The particles were incubated in simulated body fluid (SBF; comprised of NaCl, $NaHCO_3$, KCl, $Na_2HPO_4{\cdot}2H_2O$, $MgCl_2{\cdot}6H_2O$, Na_2SO_4, $(CH_2OH)_3CNH_2$, $CaCl_2{\cdot}2H_2O$, and HCl) [22–24] containing 2 mg·ml^{-1} doxorubicin (DOX) as model drug with water solubility of 1.18 mg·ml^{-1} [25] for 12, 24, 36, or 48 h in order to determine the minimum immersion interval that

provides the statistically maximum drug encapsulation (E_m). The solution was further centrifuged at 16,100 rcf for 10 min to separate the DOX-loaded nanoparticles from the supernatant. The DOX content of the supernatant was further measured via comparing its obtained UV-Vis spectrum with that of a reference solution comprising 2 mg·ml^{-1} of this chemotherapeutic agent.

Drug release

The drug release studies were carried out following stabilization of 2 mg·ml^{-1} of the DOX-loaded nanoparticles in SBF for 7 days at 37 °C. The amount of drug leakage was measured via comparison of the UV-Vis spectrum of the supernatant with that of a reference solution comprising E_m mg·ml^{-1} of DOX. The drug release ratios at increased temperatures were performed for 30 min at 10 different temperatures ranging from 30 °C to 75 °C in a waterbath until no statistically significant increase in the drug release ratio was observed. After the heat treatments, the PEG1500-PMNPs were separated from the supernatants and the drug contents of the supernatants were measured by UV-Vis technique.

Hyperthermia experiments

The hyperthermia conditions were achieved by MRgFUS (EX-ablate, Insightec, Haifa, Israel) and magnetic hyperthermia (Easyheat 3542LI, 4 kW, Ambrell, Gloucestershire, UK). A typical MRgFUS procedure used for sonication of tissue-mimicking phantoms containing DOX-loaded nanostructures is shown in Figure 2. The drug-loaded PEG1500-PMNPs (1 mg·ml^{-1}) were firstly incorporated in a thermosensitive tissue-mimicking phantom [26] and sonicated for 5 × 20 s using an acoustic energy of approximately 500 J, acoustic power of 25 W, and frequency of 1.15 MHz. The minimum temperature range within the focal region (with around 2 mm size) was approximately 43–46 °C according to the obtained time–temperature profiles.

A schematic of the experimental setup employed for the magnetic hyperthermia investigations is shown in Figure 3. The magnetic field was generated by a helical coil with 8 turns and inner diameter of 2.54 cm. Three different experimental conditions (Table 1) were examined to determine the optimal range of AMF strength which results in temperatures above the melting point of PEG1500. The magnetic field

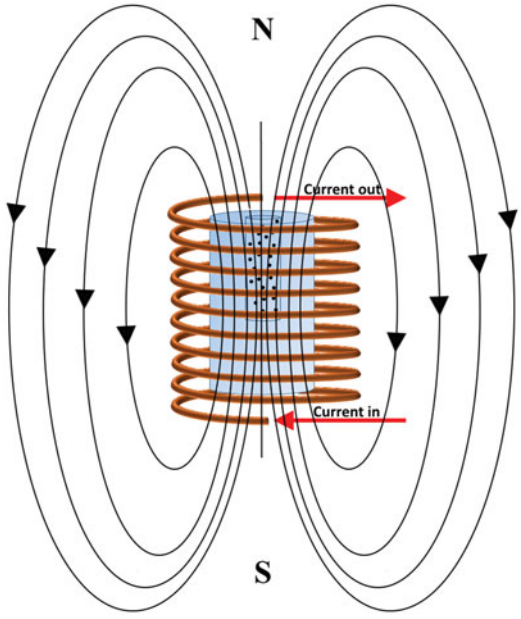

Figure 3. A schematic of the approach used for heating the solution containing superparamagnetic nanoparticles under exposure to an AMF. The tube containing SBF solution and nanoparticles was embedded in a tissue-mimicking phantom and exposed to the AMF with different experimental parameters.

Table 1. The experimental characteristics applied in the magnetic nanoparticle hyperthermia tests.

Concentration (mg·ml^{-1})	Time (min)	Current (A)	Frequency (KHz)	Power (W)	Field strength (kA·m^{-1})
1	90	100	318	77-92	31.5
1	90	150	313	325-350	47.2
1	90	200	312	715-740	63.0

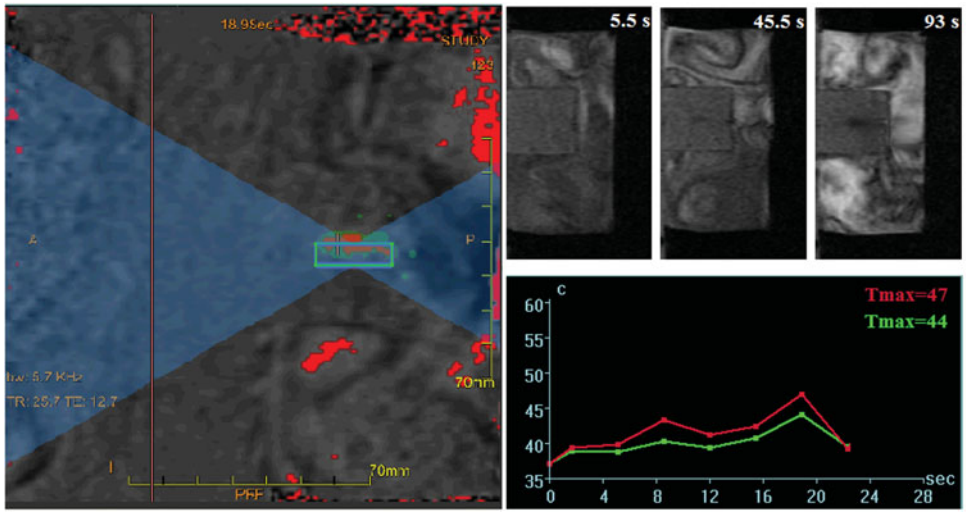

Figure 2. A typical HIFU procedure performed for sonication of a tissue-mimicking phantom containing superparamagnetic nanoparticles. Formation of a dark area around the particles container in the tissue-mimicking phantom indicated partial melting of the polymer and exposure of the magnetic core.

strengths (H) generated at various experimental currents were determined using Equation (1):

$$H = \frac{ni}{L} \quad (1)$$

where n, i, and L represent the coil turns, current (A), and inner coil diameter (m). The specific absorption rate (SAR) of the nanoparticles was also calculated using Equation (2) [27–30]:

$$\mathrm{SAR} = C_m \frac{M_m}{M_P}\left(\frac{\Delta T}{\Delta t}\right) \quad (2)$$

where M_m and M_p are respectively the medium and nanoparticles weights, C_m is the specific heat capacity of the medium (4.127 $J{\cdot}g^{-1}{\cdot}K^{-1}$), and ΔT represents the temperature rise in a particular time interval (Δt). After the heat treatments, the particles were centrifuged and the drug release ratio was quantified through comparing the UV-Vis spectra of the supernatants with that of the reference solution.

Cytotoxicity assays

The cell viability investigations were carried out using human lung adenocarcinoma (A549) grown in RPMI1640 media (Roswell Park Memorial Institute) supplemented with 10% fetal bovine serum and 1% penicillin/streptomycin in a humidified incubator with 5% CO_2 at 37 °C [31–33].

The cytotoxic effects of the PEG1500-PMNPs, DOX-loaded PEG1500-PMNPs, and free DOX were quantified using a (3–(4,5-Dimethylthiazol-2-yl)-2,5-Diphenyltetrazolium Bromide) (MTT) assay [34,35]. The cells were cultivated with 100 µl RPMI1640 in a 96-well plate at a density of 5×10^4 cells·ml^{-1}, followed by 24-h incubation to allow cell adherence to the plate surface. After the addition of phosphate buffered saline (PBS) containing pre-defined concentrations of PEG1500-PMNPs, DOX-PEG1500-PMNPs, and free DOX, the A549 cells were again incubated for 24, 48, and 72 h, followed by replacement of the media, incubation of the cells in a fresh medium for 24 h, removal of the media, and adding 50 µl of the MTT reagent. After incubation at 37 °C for 4.5 h, 100 µl of pure dimethylsulfoxide was added and left in the dark for 30 min to dissolve the crystal formazan. Then, 25 ml Sorensen's glycine buffer was added and the absorbance was detected at 570 nm with a microplate absorbance reader (Multiskan, ThermoScientific, Madison, WI). The cytotoxicity was reported as the ratio of the viable A549 cells compared to the control well.

The proliferation of A549 cells were also assessed by CellReporter™ (Molecular Devices LLC, Sunnyvale, CA) using 4′,6-diamidino-2-phenylindole (DAPI; Sigma-Aldrich, St. Louis, MO) for staining the cells nuclei.

Magnetic hyperthermia on the A549 cells

The A549 cells with population of 2×10^5 cells·ml^{-1} were seeded in a 96-well plate. After 24 h, each well was treated with either the medium, PEG1500-PMNPs, DOX-PEG1500-PMNPs, or free DOX with pre-defined concentrations. The magnetic hyperthermia tests were carried out using a 94.5 kA·m^{-1} field for 2 h. The samples media were replaced after 6 or 48 h and then, the cells were harvested and plated in a 96-well plate. The MTT assay was carried out after 24 h in order to compare the cell viabilities of different test groups.

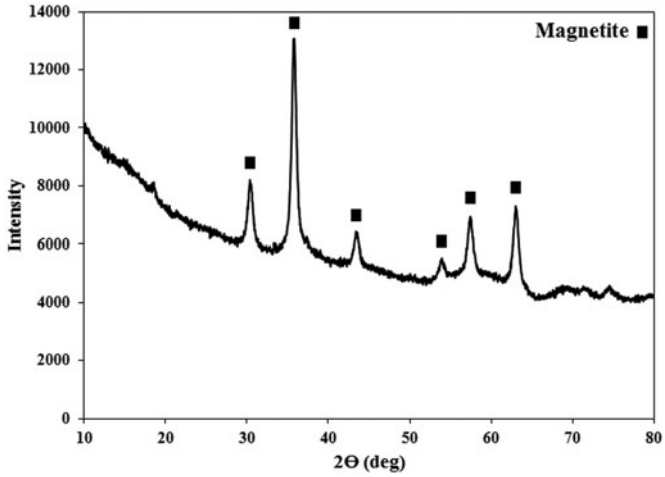

Figure 4. The XRD spectrum of the synthesized PEG1500-PMNPs. The obtained peaks confirmed formation of magnetite phase with cubic structure. A wide stretch at left side of the spectrum also showed the presence of amorphous polymeric phase.

Data analyses

The experiments were repeated for at least three times and the obtained values were reported as mean ± standard deviation (mean ± SD) using Statistical Package for Social Sciences software (SPSS; version 20, SPSS Inc., Chicago, IL, USA).

Results and discussion

Characterization

The XRD spectrum of the synthesized PMNPs (Figure 4) confirmed formation of the cubic magnetite phase (ICDD-JCPDS 00–001-1111), where the peaks at 2θ of 30, 35, 43, 54, 57, and 63 degrees, respectively corresponded to the (220), (311), (400), (422), (511), and (440) planes of the magnetite lattice structure. The observed stretch at low 2θ angles of the XRD pattern was possibly attributed to the amorphous PEG phase generated as the protective shell around the PMNP cores.

The FT-IR spectra of the diamine-terminated PEG, PMNPs, and PEG1500-PMNPs are shown in Figure 5. The characteristic peaks of both PEG1500 and PMNPs were detected in the FT-IR spectrum of PEG1500-PMNPs. However, the significantly higher intensities of the PMNP peaks showed the dominance of its weight fraction in the nanoparticle structure.

The TEM image of the synthesized PMNPs is shown in Figure 6(a). Incorporation of CTAB into the reaction mixture resulted in the formation of large aggregated nanostructures with diameters of around 175 nm, mainly composed of smaller nanoparticles with approximately 10 nm diameters rather than the generation of a mesoporous structure. This

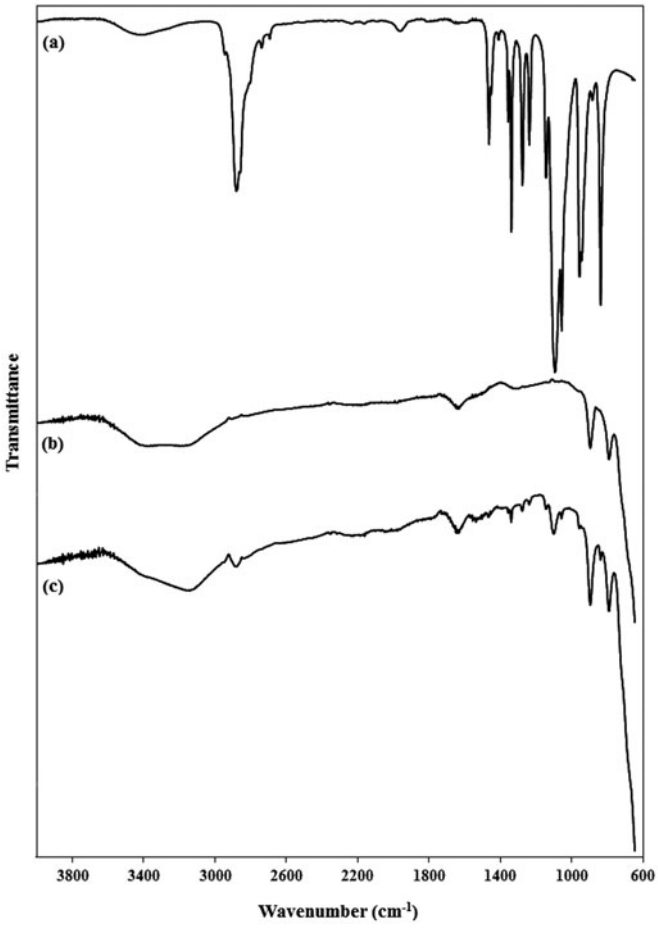

Figure 5. FTIR spectra of (a) PEG1500, (b) pure PMNPs, and (c) PEG1500-PMNPs. The main peaks of both PEG1500 and PMNPs were observed in the FTIR spectrum of PEG1500-PMNPs.

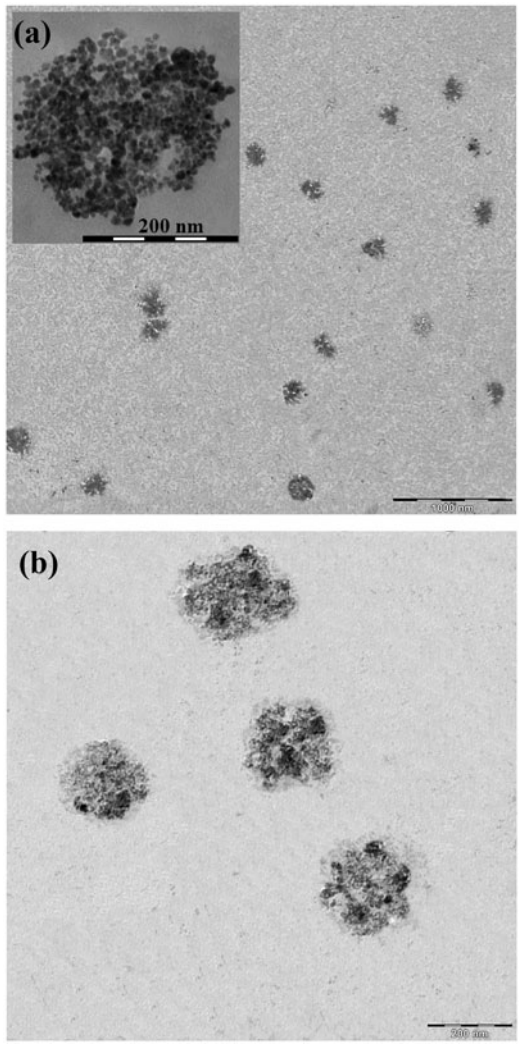

Figure 6. TEM image of the synthesized (a) PMNPs and (b) PEG1500-PMNPs. A thin polymeric nanoshell is observed on the surfaces of PEG1500-PMNPs.

could be probably due to a relatively small size of the single MNPs, which led to the formation of aggregates around the polar terminals of the surfactant, rather than well-defined tubular arrays observed in the mesoporous structures such as mesoporous silica nanoparticles (MSNs). However, the presence of interparticle porosities in these large aggregates could further enhance the drug encapsulation capacity of the PMNPs. The TEM image of the PMNPs coated by PEG1500 (Figure 6(b)) also showed a thin layer of polymer coating with uniform thickness around the agglomerated nanoparticles, which could potentially protect the encapsulated drug from premature leakage at temperature ranges lower than its melting temperature.

The morphological investigations by Image J software indicated the formation of a polymer coating with approximately 4 nm thickness around the porous nanoparticles. The TGA analysis of PEG1500-PMNPs (Figure 7(a)) also exhibited a sharp weight loss at temperatures below 100 °C, possibly due to the water evaporation from the porous nanostructures. The secondary phase of weight loss (approximately 6%) at temperature range of 270–300 °C represented the weight proportion of the PEG1500 coating.

The phase transition behavior of the PEG1500-PMNPs investigated by DSC technique is shown in Figure 7(b). The obtained spectrum indicated a peak phase transition at 48 ± 2 °C, corresponding to the melting point of the PEG1500 shell. However, the onset temperature of phase transition observed at 40 ± 2 °C confirmed the suitability of PEG1500 for drug release under hyperthermia condition. The obtained values of onset and peak temperatures of phase transition were almost equal to those of pure PEG1500 and thus, the phase transition behavior of this polymer was not affected by its conjugation to the PMNP surfaces.

The magnetization curves of the as-synthesized PMNPs as well as PEG1500-PMNPs at room temperature are illustrated in Figure 8. In spite of the increased particle size, the hysteresis and coercivity of the synthesized PMNPs were surprisingly negligible, probably due to the particular morphology of the aggregates which are consisted of numerous MNPs with average size of approximately 10 nm and superparamagnetic behavior. Formation of the polymer layer later decreased the specific magnetization value from 49 ± 3 to 34 ± 5 emu·g^{-1}, most likely due to the diamagnetic nature of the polymeric nanoshell [36] as well as disordered surface spins [37], whereas no significant alteration was detected in the hysteresis and coercivity values of the nanostructures.

The thermal profiles of the SBF solution containing 1 mg·ml^{-1} of PEG1500-PMNPs at various AMF strengths are shown in Figure 9. The gradual heating of the solution for

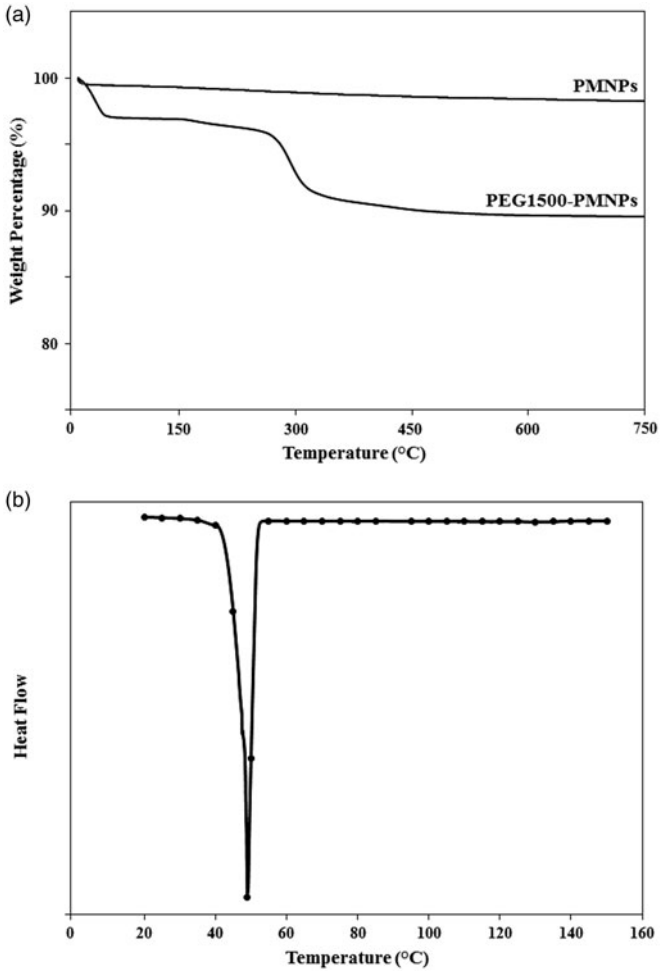

Figure 7. (a) The TGA and (b) DSC analyses of the synthesized PEG1500-PMNPs.

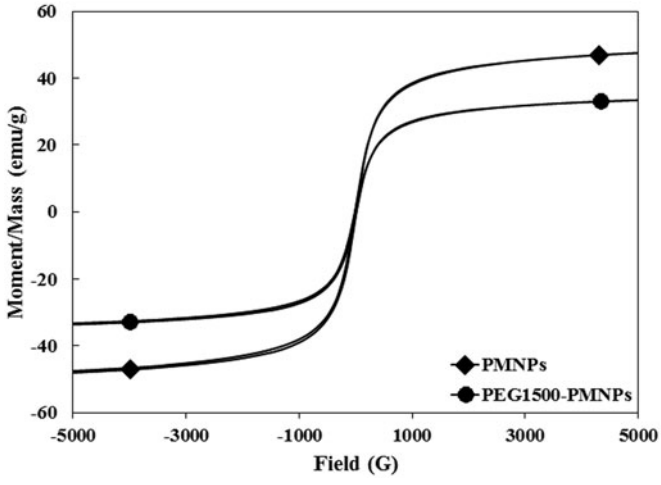

Figure 8. The magnetization curves of PMNPs and PEG1500-PMNPs. In spite of a significant increase of their size, the coercivity values of both PMNPs and PEG1500-PMNPs were near to zero.

15 min resulted in maximum temperature of 40 ± 2 °C, 43 ± 3 °C, and 50 ± 2 °C when the field strengths of 31.5 kA·m^{-1}, 47.2 kA·m^{-1}, and 63.0 kA·m^{-1}, respectively were applied and then, no statistically significant temperature rise over time was observed in all three studied AMF strengths. Therefore, the heating interval of 15 min and AMF strength

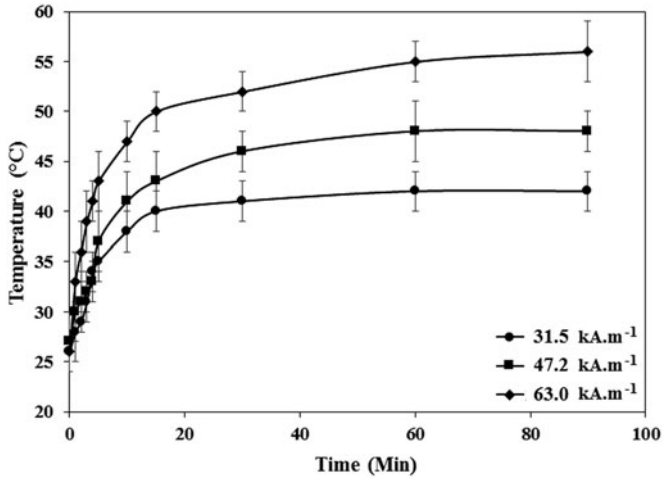

Figure 9. The temperature profiles of the SBF solutions containing PEG1500-PMNPs obtained after exposure to the AMF with varied strengths and different durations. The time of 15 min was found as the optimal interval for all three selected field strengths. However, the 63.0 kA·m^{-1} AMF could only provide a temperature above melting point of PEG1500 at this interval.

Table 2. The morphological/physical characteristics of PMNPs and PEG1500-PMNPs as well as the drug loading/release behavior of PEG1500-PMNPs.

	PMNPs	PEG1500-PMNPs
Particle size (nm)	175 ± 72	179 ± 90
Zeta potential (mV)	−25.8 ± 1.4	−5.5 ± 0.9
Surface area (m^2·g^{-1})	91 ± 17	35 ± 12
Specific magnetization (emu·g^{-1})	49 ± 3	34 ± 5
Drug Encapsulation (mg·g^{-1})	–	235 ± 26
Maximum waterbath drug release (%)	–	71 ± 4
HIFU drug release (%)	–	48 ± 3
Magnetic hyperthermia drug release (%)	–	74 ± 5

of 47.2 kA·m^{-1} were considered as the minimum heating intervals and AMF strengths which could generate temperatures above the melting point of PEG1500. The maximum reachable temperatures after exposure to the AMF for 90 min with 31.5 kA·m^{-1}, 47.2 kA·m^{-1}, and 63.0 kA·m^{-1}, respectively were 42 ± 2 °C, 48 ± 2 °C, and 56 ± 3 °C. The obtained SAR values for different AMF strengths were also 120.4 W·g^{-1}, 172.0 W·g^{-1}, and 206.3 W·g^{-1}.

Various morphological and physical properties of PMNPs and PEG1500-PMNPs are summarized in Table 2. Addition of CTAB to the synthesis solution resulted in a significant increase in the particle size from 10 nm [20] to 175 nm, which was further increased to 179 nm after formation of the PEG1500 nanoshell. However, the PEG1500 layer decreased the particles zeta potential, leading to increased agglomeration vulnerability at physiological environments. Moreover, the formation of the PEG1500 layer caused a threefold decrease of the surface area, due to coverage of the large particle aggregates and limited accessibility to the small MNP surfaces.

Drug loading

Measurement of the drug loading capacity of PEG1500-PMNPs indicated an incubation time of 36 h as the optimal encapsulation interval, resulting in 235 ± 26 mg of DOX

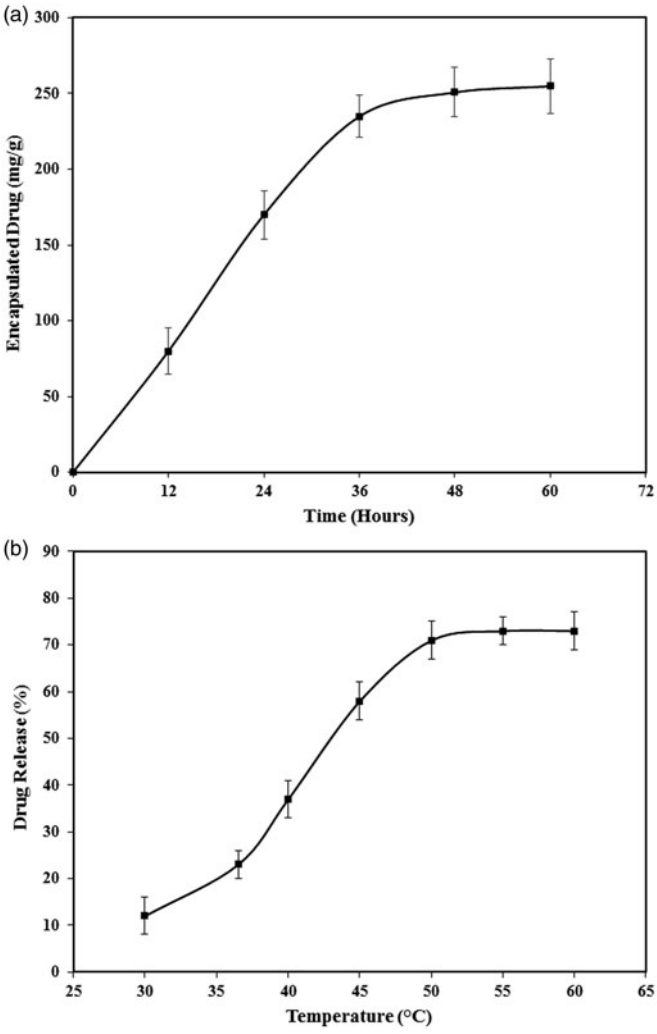

Figure 10. The nanoparticles ability in (a) encapsulation and (b) release of DOX used as a model drug.

loaded on 1 g PEG1500-PMNPs (Figure 10(a)). This incubation time is significantly less than that obtained in the previous study (48 h) where MSNs were used as the reservoir cores, probably due to larger pore size of the PMNPs compared to those observed in MSNs and thus, easier penetration of the aqueous solution into the core structure [8,14]. The obtained loading capacity is also comparable to that reported for other porous drug carriers such as MSNs [8,14]. Therefore, this incubation time was utilized in further steps for encapsulation of DOX into the PEG1500-PMNPs.

Drug release

Investigation of the drug release behavior of the DOX-PEG1500-PMNPs at elevated temperatures showed their potential for rapid unloading of their cargo at various hyperthermia conditions. The maximum measured ratio of DOX release was 70 ± 4%, achieved after heating at 50 °C for 30 min in a waterbath and then, no significant increase in the DOX release ratio was observed by further heating of the nanoparticles at higher temperatures (Figure 10(b)). However, the ratio of DOX leakage during stabilization of DOX-PEG-PMNPs at 37 °C was relatively high (21 ± 4%), most likely due

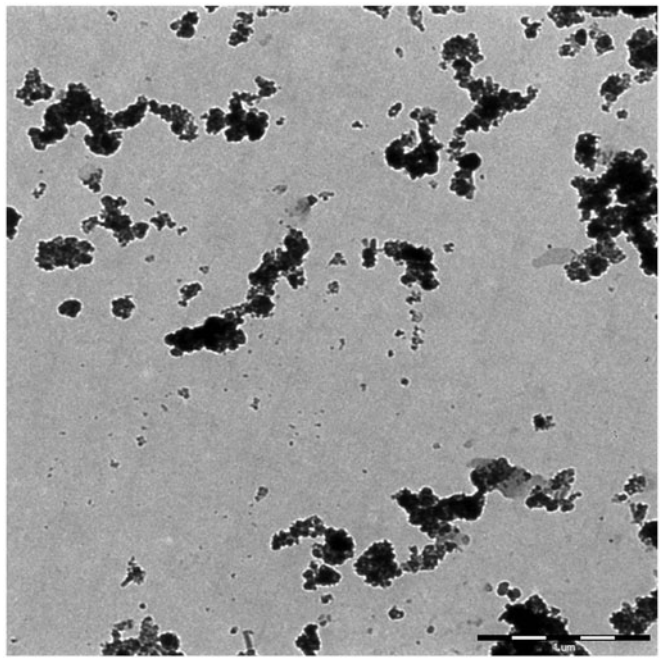

Figure 11. A typical TEM image of PEG1500-PMNPs after heating at 50 °C. Melting of the polymeric shell resulted in formation of large nanoparticle aggregates in the solution. Numerous individual nanoparticles detached from the initial agglomerates were also observed in the solution.

to the low thickness of the protective PEG1500 shell. The statistical analyses showed no significant difference between the ratio of DOX leakage during stabilization and that released after heating in waterbath at 37 °C for 30 min (23 ± 3%), which indicated a rapid leakage of approximately 20% of the encapsulated DOX upon addition of the nanoparticles to the medium.

In order to provide more realistic conditions for evaluation of the drug release behavior of the DOX-PEG1500-PMNPs, the nanoparticles were also exposed to MRgFUS sonication for 100 s as well as a 63.0 kA·m^{-1} AMF for 15 min, which both generated temperatures around 48–50 °C in the media. Investigation of the drug release ratios after heating by these hyperthermia modalities indicated the high potential of DOX-PEG1500-PMNPs for controlled release of a considerable amount of the encapsulated drug, where MRgFUS sonication and AMF irradiation led to 48 ± 3% and 74 ± 5% DOX release in the SBF solution, respectively. A higher drug release ratio obtained by magnetic nanoparticle hyperthermia compared to MRgFUS sonication could be attributed to its higher time interval as well as the positive effect of magnetic field on the heating efficacy of PMNPs and consequently, on the melting kinetics of the PEG1500 nanoshell.

A typical TEM image of the PEG1500-PMNP nanoparticles after heating by a 63.0 kA·m^{-1} AMF is shown in Figure 11. A high degree of agglomeration was observed in the nanoparticles, mostly due to melting or gelation of the polymeric nanoshell. Moreover, exposure to the AMF resulted in partial detachment of individual MNPs from the agglomerates, probably due to their intensive vibrational motions under the AMF exposure. Therefore, dissociation of the polymeric shell and detachment of the single MNPs from the larger aggregates after heating could provide preferred routes for

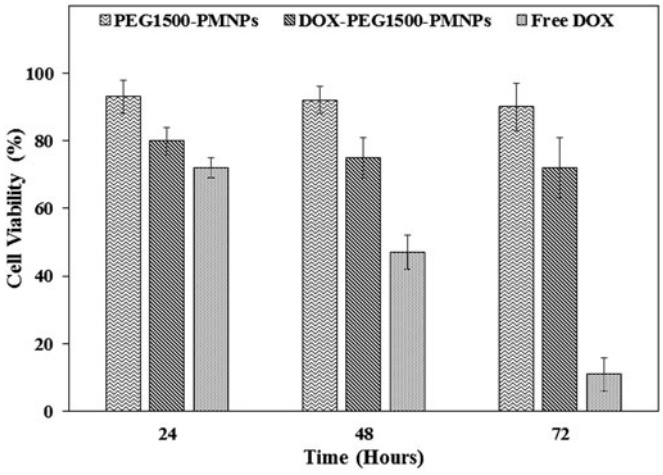

Figure 12. The cytotoxic effects exerted by 160 μg·ml^{-1} PEG1500-PMNPs, 30 μg·ml^{-1} free DOX, and 200 μg·ml^{-1} DOX-PEG1500-PMNPs against the A549 cells after 24, 48, and 72 h.

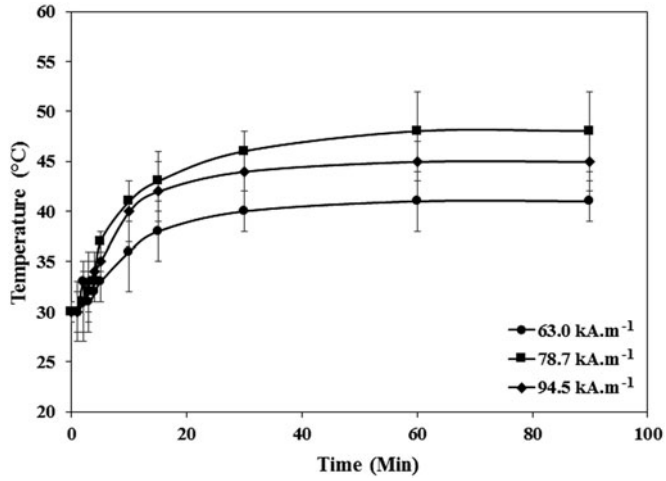

Figure 13. The temperature profiles of the media containing 160 μg·ml^{-1} PEG1500-PMNPs obtained after exposure to the AMF with varied strengths and durations. The minimum field strength required to achieve temperatures above the PEG1500 melting point was 94.5 kA·m^{-1}.

controlled drug release from the nanostructure into the target tissue.

Cytotoxicity assays

The nanoparticles concentrations used in the MTT assays were calculated based on the preliminary studies which showed that 200 μg·ml^{-1} DOX-PEG1500-PMNPs was the minimal concentration needed to achieve temperatures above the PEG1500 melting point using AMF strengths below 100 kA·m^{-1}. According to the drug loading and release results, this amount of DOX-PEG1500-PMNPs is composed of approximately 160 μg·ml^{-1} PEG1500-PMNPs and 40 μg·ml^{-1} DOX, which could release around 30 μg·ml^{-1} of its DOX content in hyperthermia condition. It is noteworthy that for obtaining the hyperthermia temperatures above the PEG1500 melting point using this concentration of nanostructures, the medium must be initially heated to 30 °C.

The cytotoxicity degrees of the PEG1500-PMNPs (160 μg·ml^{-1}), DOX-PEG1500-PMNPs (200 μg·ml^{-1}), and free DOX (30 μg·ml^{-1}) were analyzed against A549 cells using the MTT assay. The obtained results shown in Figure 12, indicated the negligible cytotoxicity of the PEG1500-PMNPs in incubation intervals of 24, 48, and 72 h. In contrast, incubation of A549 cells with free DOX led to 28%, 53%, and 89% reduction of the cell viability after 24, 48, and 72 h, respectively. Although the concentration of free DOX applied in this study was significantly higher than its half maximal inhibitory concentration (IC50), a relatively low cytotoxicity was observed at the initial 24 h, probably due to the genetic polymorphism, which its manifestation in the used A549 cell lines may translate to reduced transportation rates of free DOX [38,39]. However, the obtained results aptly indicated the significant cytotoxicity of free DOX at increased intervals, where the cell viability ratio reached approximately 10% after 72 h. In contrast, when the DOX-PEG1500-PMNPs were added, the cell viability was reduced to 20%, 25%, and 28% for incubation intervals of 24, 48, and 72 h, which again indicated the rapid partial leakage of the encapsulated DOX within the medium.

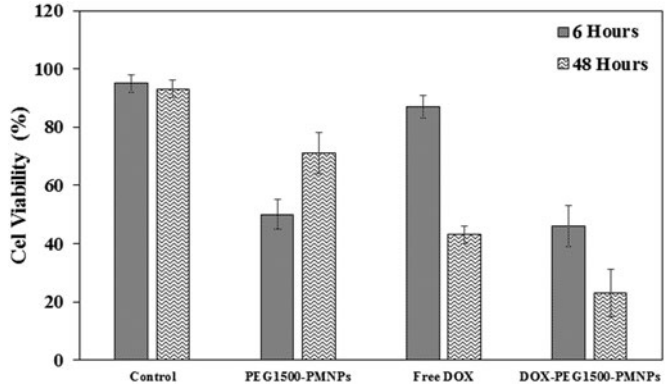

Figure 14. The cell viability ratios of the control A549 cells and those treated with 160 μg·ml^{-1} PEG1500-PMNPs, 30 μg·ml^{-1} free DOX, and 200 μg·ml^{-1} DOX-PEG1500-PMNPs after exposure to the magnetic hyperthermia condition.

In vitro hyperthermia under AMF exposure

The temperature profiles obtained by exposure of 160 μg·ml^{-1} PEG1500-PMNPs to different AMF strengths are presented in Figure 13. The minimal AMF strength required to achieve temperatures above the PEG1500 melting point was 94.5 kA·m^{-1}, which is significantly higher than the clinical safety limit of 13 kA·m^{-1}. However, the AMF strength required to melt the polymeric shell could be reduced in further studies by replacing the magnetite core with Zn.Fe.O or Co.Mn.Fe.O hard-soft mixed ferrites, which can present the SAR values of above 500 W·g^{-1} at clinically relevant AMF strengths [40].

The cell viability ratios after hyperthermia treatment of the A549 cells with PEG1500-PMNPs, Free DOX, and DOX-PEG1500-PMNPs in contrast to the control group are shown in Figure 14. The viability ratios of A549 cells exposed to PEG1500-PMNPs and free DOX for 6 h were 50 ± 5% and 87 ± 4%, respectively, indicating the higher cytotoxic effect of hyperthermia treatment using 160 μg·ml^{-1} of PEG1500-PMNPs compared to 30 μg·ml^{-1} of DOX in short treatment times. However, when the media were replaced after 48 h, the viability ratio of the A549 cells treated by

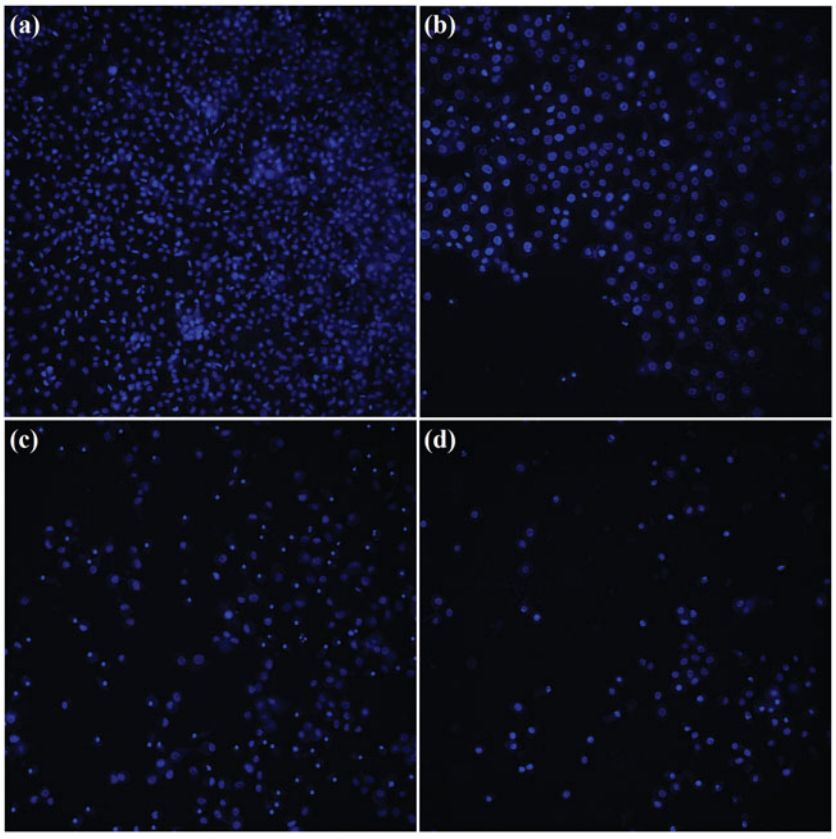

Figure 15. The CellReporter images of the stained A549 cells after hyperthermia treatments. (a) Control, (b) PEG1500-PMNPs, (c) free DOX, and (d) DOX-PEG1500-PMNPs.

PEG1500-PMNPs was increased to 71 ± 7%, while treatment with fee DOX led to 43 ± 3% cell viability. Therefore, in spite of a relatively higher capability of the magnetic hyperthermia treatment for killing the cancer cells in short treatment intervals, incomplete killing and rapid regrowth of the cells after elimination of the hyperthermia condition, result in inferior long-term efficacies compared to the chemotherapy treatment.

On the other hand, hyperthermia treatment of the A549 cells using 200 μg·ml^{-1} of DOX-PEG1500-PMNPs resulted in cell viabilities of 46 ± 7% and 23 ± 8% after 6 and 48 h. As a result of dual treatment using these thermosensitive nanocarriers, the cell viability was significantly decreased in both short and long treatment intervals attributed to magnetic hyperthermia and chemotherapy, respectively. The CellReporter images presented in Figure 15 also confirmed that the cytotoxic effect exerted by DOX-PEG1500-PMNPs after 48 h was significantly higher than those of free DOX and PEG1500-PMNPs, indicating the synergistic effect of chemotherapy and hyperthermia induced by DOX and PEG1500-PMNPs, respectively.

Conclusion

A clinically insufficient encapsulation capacity of superparamagnetic nanoparticles is their crucial limitation for application in targeted drug delivery systems. In this study, we synthesized MNPs with porous structures to obtain higher loading capacities combined with intrinsic advantages of their superparamagnetic behavior. The synthesized nanoparticles were also covered by a thin PEG1500 layer with onset melting temperature 40 ± 2 °C to endow thermal-triggered drug release capability under hyperthermia condition. When these nanocarriers were exposed to an external magnetic field with sufficient strength, the thermal energy generated in the superparamagnetic cores resulted in rapid melting of the protective PEG1500 shell at hyperthermia temperatures, thus providing preferred routes for drug diffusion into the surrounding environment. Therefore, by targeted delivery of these carriers and simultaneous utilization of an external magnetic field with proper strength, relatively higher ratios of localized delivery and lower systemic toxicity levels with improved efficacy at hyperthermia condition could be obtained. The *in vitro* cytotoxicity tests on the A549 cells further indicated that the DOX-PEG1500-PMNPs could induce enhanced cell killing via a double effect of hyperthermia and chemotherapy. However, the animal studies under the magnetic nanoparticle hyperthermia must be carried out to determine the in vivo efficiency of these carriers.

Disclosure statement

The authors have no conflicts of interest to disclose.

Funding

This work was supported by LRGS NanoMite University of Malaya [Grant No: RU029-2014] and University of Malaya Research Grant Scheme [Grant no.: RP042A-17AET].

ORCID

Ali Dabbagh http://orcid.org/0000-0002-5940-8882
Ziba Hedayatnasab http://orcid.org/0000-0002-4796-7978
Hamed Karimian http://orcid.org/0000-0002-8501-9864
Chai Hong Yeong http://orcid.org/0000-0003-1572-4143
Hamid Reza Madaah Hosseini http://orcid.org/0000-0002-5865-052X
Noor Hayaty Abu Kasim http://orcid.org/0000-0002-8889-842X
Tin Wui Wong http://orcid.org/0000-0002-9131-6937
Noorsaadah Abdul Rahman http://orcid.org/0000-0001-5847-8961

References

[1] Ghosh R, Pradhan L, Devi YP, et al. Induction heating studies of Fe_3O_4 magnetic nanoparticles capped with oleic acid and polyethylene glycol for hyperthermia. J Mater Chem. 2011;21:13388–13398.
[2] Sato I, Umemura M, Mitsudo K, et al. Simultaneous hyperthermia-chemotherapy with controlled drug delivery using single-drug nanoparticles. Sci Rep. 2016;6:24629.
[3] Quinto CA, Mohindra P, Tong S, et al. Multifunctional superparamagnetic iron oxide nanoparticles for combined chemotherapy and hyperthermia cancer treatment. Nanoscale. 2015;7:12728–12736.
[4] Liang Z, Li X, Xie Y, et al. Smart gold nanoshells for combined cancer chemotherapy and hyperthermia. Biomed Mater. 2014;9:025012.
[5] Nehate C, Aji Alex MR, Kumar A, et al. Combinatorial delivery of superparamagnetic iron oxide nanoparticles (γFe2O3) and doxorubicin using folate conjugated redox sensitive multiblock polymeric nanocarriers for enhancing the chemotherapeutic efficacy in cancer cells. Mater Sci Eng C Mater Biol Appl. 2017;75:1128–1143.
[6] Dennis CL, Ivkov R. Physics of heat generation using magnetic nanoparticles for hyperthermia. Int J Hyperthermia. 2013;29:715–729.
[7] Dabbagh A, Abdullah BJJ, Abdullah H, et al. Triggering mechanisms of thermosensitive nanoparticles under hyperthermia condition. J Pharm Sci. 2015;104:2414–2428.
[8] Dabbagh A, Mahmoodian R, Abdullah BJJ, et al. Low-melting-point polymeric nanoshells for thermal-triggered drug release under hyperthermia condition. Int J Hyperthermia. 2015;31:920–929.
[9] Revia RA, Zhang M. Magnetite nanoparticles for cancer diagnosis, treatment, and treatment monitoring: recent advances. Mater Today (Kidlington). 2016;19:157–168.
[10] Luo C, Sun J, Liu D, et al. Self-assembled redox dual-responsive prodrug-nanosystem formed by single thioether-bridged paclitaxel-fatty acid conjugate for cancer chemotherapy. Nano Lett. 2016;16:5401–5408.
[11] Saffari M, Ebrahimi A, Langrish T. A novel formulation for solubility and content uniformity enhancement of poorly water-soluble drugs using highly-porous mannitol. Eur J Pharm Sci. 2016;83:52–61.
[12] Tamarov K, Xu W, Osminkina L, et al. Temperature responsive porous silicon nanoparticles for cancer therapy - spatiotemporal triggering through infrared and radiofrequency electromagnetic heating. J Control Release. 2016;241:220–228.
[13] Gedda G, Pandey S, Khan MS, et al. Synthesis of mesoporous titanium oxide for release control and high efficiency drug delivery of vinorelbine bitartrate. RSC Adv. 2016;6:13145–13151.
[14] Dabbagh A, Abdullah BJJ, Abu Kasim NH, et al. A new mechanism of thermal sensitivity for rapid drug release and low systemic toxicity in hyperthermia and thermal ablation temperature ranges. Int J Hyperthermia. 2015;31:375–385.
[15] Zhang J, Misra RDK. Magnetic drug-targeting carrier encapsulated with thermosensitive smart polymer: core–shell nanoparticle carrier and drug release response. Acta Biomater. 2007;3:838–850.
[16] Iqbal M, Robin S, Humbert P, et al. Submicron polycaprolactone particles as a carrier for imaging contrast agent for in vitro applications. Colloids Surf B Biointerfaces. 2015;136:488–495.
[17] Wen H, Dong C, Dong H, et al. Engineered redox-responsive PEG detachment mechanism in PEGylated nano-graphene oxide for intracellular drug delivery. Small. 2012;8:760–769.
[18] Takae S, Miyata K, Oba M, et al. PEG-detachable polyplex micelles based on disulfide-linked block catiomers as bioresponsive nonviral gene vectors. J Am Chem Soc. 2008;130:6001–6009.
[19] Thamphiwatana S, Fu V, Zhu J, et al. Nanoparticle-stabilized liposomes for pH-responsive gastric drug delivery. Langmuir. 2013;29:12228–12233.
[20] Dabbagh A, Abu Kasim NH, Bakri MM, et al. Polyethylene-glycol coated maghemite nanoparticles for treatment of dental hypersensitivity. Mater Lett. 2014; 4/15/121:89–92.
[21] Gil S, Castro E, Mano JF. Synthesis and characterization of stable dicarboxylic pegylated magnetite nanoparticles. Mater Lett. 2013;100:266–270.
[22] Sarraf M, Razak BA, Nasiri-Tabrizi B, et al. Nanomechanical properties, wear resistance and in-vitro characterization of Ta2O5 nanotubes coating on biomedical grade Ti-6Al-4V. J Mech Behav Biomed Mater. 2017;66:159–171.
[23] Sarraf M, Dabbagh A, Abdul Razak B, et al. Silver oxide nanoparticles-decorated tantala nanotubes for enhanced antibacterial activity and osseointegration of Ti6Al4V. Mater Des. 2018;154:28–40.
[24] Sarraf M, Dabbagh A, Abdul Razak B, et al. Highly-ordered TiO_2 nanotubes decorated with Ag_2O nanoparticles for improved biofunctionality of Ti6Al4V. Surf Coat Technol. 2018;349:1008–1017.
[25] Dabbagh A, Abu Kasim NH, Yeong CH, et al. Critical parameters for particle-based pulmonary delivery of chemotherapeutics. J Aerosol Med Pulm Drug Deliv. 2018;31:139–154.
[26] Dabbagh A, Abdullah BJ, Abu Kasim NH, et al. Reusable heat-sensitive phantom for precise estimation of thermal profile in hyperthermia application. Int J Hyperthermia. 2014;30:66–74.
[27] Salas G, Veintemillas-Verdaguer S, Morales MP. Relationship between physico-chemical properties of magnetic fluids and their heating capacity. Int J Hyperthermia. 2013;29:768–776.
[28] LeBrun A, Manuchehrabadi N, Attaluri A, et al. MicroCT image-generated tumour geometry and SAR distribution for tumour temperature elevation simulations in magnetic nanoparticle hyperthermia. Int J Hyperthermia. 2013;29:730–738.
[29] Oliveira TR, Stauffer PR, Lee C-T, et al. Magnetic fluid hyperthermia for bladder cancer: A preclinical dosimetry study. Int J Hyperthermia. 2013;29:835–844.
[30] Eneko G, Olivier S, Juan-Mari C, et al. Specific absorption rate dependence on temperature in magnetic field hyperthermia measured by dynamic hysteresis losses (ac magnetometry). Nanotechnology. 2015;26:015704.
[31] Akbarzadeh A, Mikaeili H, Zarghami N, et al. Preparation and in vitro evaluation of doxorubicin-loaded Fe3O4 magnetic nanoparticles modified with biocompatible copolymers. Int J Nanomedicine. 2012;7:511–526.
[32] Kim HC, Kim E, Jeong SW, et al. Magnetic nanoparticle-conjugated polymeric micelles for combined hyperthermia and chemotherapy. Nanoscale. 2015;7:16470–16480.
[33] Rosman R, Saifullah B, Maniam S, et al. Improved anticancer effect of magnetite nanocomposite formulation of GALLIC Acid (Fe(3)O(4)-PEG-GA) against lung, breast and colon cancer cells. Nanomaterials. 2018;8:83.
[34] Karimian H, Mohan S, Moghadamtousi S, et al. Tanacetum polycephalum (L.) Schultz-Bip. induces mitochondrial-mediated apoptosis and inhibits migration and invasion in MCF7 cells. Molecules. 2014;19:9478–9501.

[35] Bindal P, Bindal U, Lin CW, et al. Neuro-fuzzy method for predicting the viability of stem cells treated at different time-concentration conditions. THC. 2017;25:1041–1051.
[36] Tai MF, Lai CW, Abdul Hamid SB. Facile synthesis polyethylene glycol coated magnetite nanoparticles for high colloidal stability. J Nanomater. 2016;2016:1.
[37] Reyes-Ortega F, Delgado ÁV, Schneider EK, et al. Magnetic nanoparticles coated with a thermosensitive polymer with hyperthermia properties. Polymers. 2018;10:10.
[38] Bray J, Sludden J, Griffin MJ, et al. Influence of pharmacogenetics on response and toxicity in breast cancer patients treated with doxorubicin and cyclophosphamide. Br J Cancer. 2010;102:1003–1009.
[39] Todorova VK, Makhoul I, Dhakal I, et al. Polymorphic variations associated with doxorubicin-induced cardiotoxicity in breast cancer patients. Oncol Res. 2017;25:1223–1229.
[40] He S, Zhang H, Liu Y, et al. Maximizing specific loss power for magnetic hyperthermia by hard–soft mixed ferrites. Small. 2018; 14:e1800135.